Spring 5-19-2018

Propagation in Synthetic Mucus: Advantages and Limitations to a Modular Approach

Louis Rogowski
Southern Methodist University, lrogowski@smu.edu

PROPAGATION IN SYNTHETIC MUCUS:
ADVANTAGES AND LIMITATIONS TO
A MODULAR APPROACH

Approved by:

Dr. MinJun Kim
Professor

Dr. Ali Beskok
Professor

Dr. Edmund Richer
Associate Professor

PROPAGATION IN SYNTHETIC MUCUS: ADVANTAGES AND LIMITATIONS TO A MODULAR APPROACH

A Masters Defense Presented to the Graduate Faculty of the

Lyle School of Engineering

Southern Methodist University

in

Partial Fulfillment of the Requirements

for the degree of

Master of Science in Mechanical Engineering

with a

Major in Mechanical Engineering

by

Louis William Rogowski

B.S., Mechanical Engineering, Drexel University, Philadelphia

May 19, 2018

ACKNOWLEDGMENTS

This work could not have been completed without the guidance of my adviser, Dr. MinJun Kim. The support of my mentors Dr. Hoyeon Kim, Dr. Jamel Ali, and Dr. U Kei Cheang. My fellow colleagues Samuel Sheckman, Xiao Zhang, Bin Peng, Jung Soo Lee, and Jugal Saharia. The members of my committee Dr. Ali Beskok and Dr. Edmund Richer. My family for supporting me through the entire endeavor. And my grandfather, for giving me the motivation to pursue graduate school.

Rogowski, Louis William B.S., Mechanical Engineering, Drexel University, Philadelphia

Propagation in Synthetic Mucus:
Advantages and Limitations to
a Modular Approach

Advisor: Dr. MinJun Kim
Master of Science in Mechanical Engineering degree conferred May 19, 2018
Masters Defense completed April 19, 2018

This paper demonstrates the performance of modular magnetic bead based microswimmers inside synthetic mucus environments. The microswimmers under investigation are composed of chemically bonded magnetic spheres and are actuated using rotating magnetic fields. While these microswimmers have been well characterized in Newtonian fluids, their viability inside biomimetic mucus environments, has not been well defined. Understanding their performance inside such environments will provide insights into how to better design microswimmers for in vivo based tasks, such as drug delivery and minimally invasive surgery. Synthetic mucus was fabricated by mixing deionized water with mucin from a porcine stomach in varying concentrations. These formulations were analyzed using a Discovery Hybrid Rheometer 3 (DHR-3) and verified to have nonlinear viscoelastic properties. SEM imaging of the formulations revealed a heterogeneous fiber network, which is common in most biological mucus environments. Three types of microswimmers were investigated: a standard three bead achiral microswimmer, a two bead snowman swimmer, and a single bead swimmer. These microswimmer derivatives were characterized through velocity vs. frequency curves and directional controllability tests.

The results of both the tests were peculiar. Three bead achiral microswimmers could not form in high concentrations of mucus and were generally unstable during experiments. However, both snowman and single bead swimmers performed beyond expectations. This is the first documented case of symmetric particle aggregates, and more importantly, single parti-

cles, swimming without any additional geometric features normally required of low Reynolds number swimming. Single particles, when actuated, were shown to have a non-linear velocity vs. frequency relationship, which was repeated through multiple trials. Snowman swimmers exhibited consistent performance and had a linear velocity relationship, but were found to be significantly slower than the single bead swimmers. Both constructs could be directed to traverse complex trajectories, but internally generated flows tended to offset their desired directions. Due to magnetic dipole differences, swarms of single particles could be directed to swim in different directions under the same control input. These results indicate that such mucus environments can facilitate swimming without additional geometric properties such as chirality or flexibility. The single bead swimmers demonstrated in this paper may very well be the simplest microswimmer that could be used for in vivo drug delivery applications.

TABLE OF CONTENTS

LIST OF FIGURES

This paper is dedicated to Dagny Taggart, the daughter of a woman who saved my life.

Chapter 1

INTRODUCTION

Microrobotics has the potential to revolutionize medical sciences and create a consortium of life saving procedures. Microrobotics has already made great strides towards performing minimally invasive surgery and targeted drug delivery [14, 20, 39]. In pursuit of these goals, several microrobots have been developed; each with their own unique means of propulsion. Some examples of these robots include acoustic streaming robots [17,21], magnetic sperm [18, 21], flagellated particles and helices [2,40,41], ferromagnetic microswimmers [7–10,19,28,33], and chemically driven robots [3,34].

$$Re = \frac{\rho u L}{\mu} \tag{1.1}$$

Typically, to swim on the microscale, non-reciprocal motion is required. The reason for this requirement can be found in the Reynolds number in equation 1.1. Where L is the length scale, u is the velocity, ρ is the density, and μ is the viscosity of the fluid. Reynolds number is dimensionless and signifies the ratio between inertial and viscous forces. Since the length scale is only a few microns, the inertia properties in the numerator are practically non-existent, causing the viscosity forces to be dominant. Typically, the Reynolds number of microrobots tend to be around 10^{-2}. This causes swimming at such a Reynolds number to be very different then swimming on the macroscale. To use Purcell's example, a scallop inserted into a microscale world, would not be able to swim due to its reliance on momentum, via the opening and closing of its mouth [29]. Since inertia does not exist, the scallop would oscillate back and forth as it carries out its opening and closing motion. To achieve non-reciprocal motion, a swimmer must possess some form of flexibility or chirality. Salmonella (SJW 1103) bacteria can swim by rotating their flexible flagella into a chiral shape [24]. For visualization as to what these flagella filaments look like, an image can be seen in Figure 1.1. Many groups

have tried to mimic these helices. One group successfully used direct laser writing to produce helical swimmers and demonstrated their ability to swim in an animal model [36]. Another group developed helical robots by templating helices naturally occurring in plants and were able to swim in blood [15]. Biotemplated microswimmers were built by combining bacterial flagella with a magnetic coating [1]. However, it was also shown that achiral structures can swim, provided they have at most 2-planes of symmetry [11]. Non-Newtonian environments evade the requirement of non-reciprocal motion due to their non-linear viscoelastic effects.

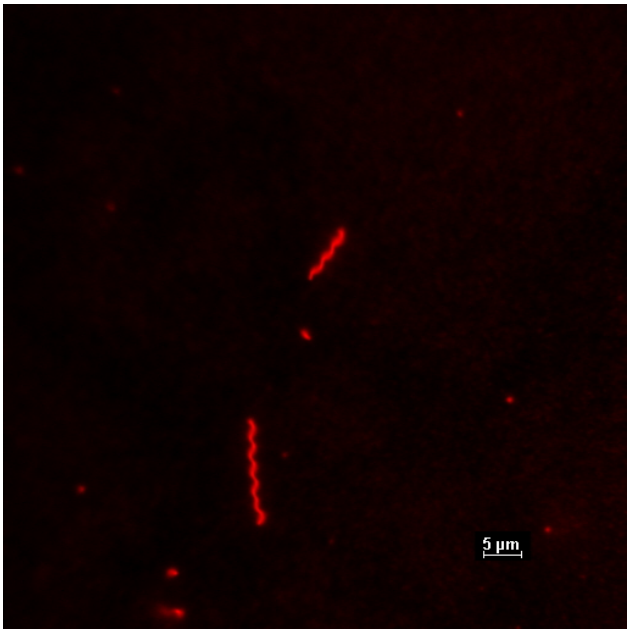

Figure 1.1. Fluorescent image of repolymerized flagella. Flagella are the primary motive force for most bacteria. Salmonella flagella are around 5-10 μm in length

Non-Newtonian fluids do not have a linear relationship with stress as shear rate increases. A Newtonian fluid, like deionized water has a purely linear relationship, and when examining its viscosity vs. shear rate curve, it would be a straight horizontal line with little variation. Some of the major subsets of non-Newtonian fluids are shear thinning, shear thickening, and viscoelastic solids. As an additional cause for complications, some fluids, like polymer fluids, have structural fiber networks embedded within them [22,24]. These structured fluidic networks contain voids that allow smaller objects in suspension to diffuse through them, while

larger objects would become trapped inside the fibrous structures. All of these properties together can create for some unique challenges and advantages to microswimmer design and implementation.

The properties that these structured fluids impart onto microswimmers can have varying effects. One group developed Nano propellers to swim through the mesh fibers of Hyaluronan (HA) solutions [35]. They found that nanoscale propellers have an advantage due to their length scale being comparable to the mesh density of the surrounding fluidic media, but larger propellers would experience hindrance in the network. Another group tested helical swimmers inside methyl cellulose (MC) solutions below concentrations of 0.5% [27]. In this case, the fluids were Newtonian but the structural nature of the fluid allowed for slight increases in swimming speed as mesh density was increased with higher concentrations of MC. This was consistent with the swimming behavior observed of bacteria when suspended in such MC concentrations [4]. One group analyzing helical swimmers found that overall, the swimming speed for a swimmer inside shear thinning fluids was always greater than Newtonian fluids. Where a higher viscosity fluid surrounds the swimmer, while as the swimmer rotates, it produces a lower viscosity region around the swimmer [16]. Another paper suggests that in fluids that experience odd viscosity, can feel additional pressure because of its swimming strokes [23]. The enhanced propulsion characteristics of heterogeneous fluids was also demonstrated in a number of other works [13, 25, 26, 32, 38]. Other groups have developed more brute force microswimmers to swim in non-Newtonian environments, such as 3D printed scallops at much larger length scales that ignore the voids within the fluid but are still able to swim purely in bulk fluid [30, 37].

This paper seeks to explore the interactions between synthetic biological environments and achiral microswimmers along with their derivative structures. The biological environment is a formulated synthetic mucus, which mimics the viscoelastic properties of human gastrointestinal mucus. The microswimmers are composed of chemically bonded magnetic particles [9, 10]. These microswimmers have been highly characterized in Newtonian fluids through feedback control [8] and close boundary conditions [7]. This paper seeks to

understand the advantages and limitations such microswimmers have inside this biological environment, and whether they are viable for in vivo applications. Conventional drug delivery systems to date have had issues becoming trapped within the mucus through either steric or adhesive forces. Some groups have developed mucus adhesive particles for drug delivery [5,31], but it is still a challenge to design drug delivery systems for such environments. By testing a more active method for drug delivery, more distributive effects may be possible. The tests performed in this paper will encompass the velocity vs. frequency response of different microswimmer derivatives, the directional responsiveness of these swimmers, and unusual side effects that come from being exposed to a biological environment. The major contributions of this paper include: 1) The inability of achiral structures to form in high concentrations of mucus 2) The ability of two bead snowman swimmers to propagate through high concentrations of mucus 3) The ability of single magnetic particles to propagate through high concentrations of mucus.

Chapter 2

Methods and Materials

2.1. Microswimmer Fabrication

Fabrication of particle microswimmers is a randomized bottom up process. Magnetic microparticles, on the scale of 4-10 μm in diameter will naturally aggregate together to form linear chains when mixed together. However, magnetic attractive forces alone are not enough to keep these linear chains together, especially when exposed to high frequency rotating magnetic fields. To compensate for this, an avidin and biotin chemical functionalization is introduced onto the surface of the particles. Particles coated with biotin will naturally bind to particles with the avidin functionalization. From a chemical perspective, one avidin molecule can accept four biotin molecules, making it one of the strongest non-covalent bonds found in nature [15]. An image of this chemical bond can be seen in Figure 2.1. This bond creates a bend in the bead chains consisting of three or more beads that gives them their achiral geometry.

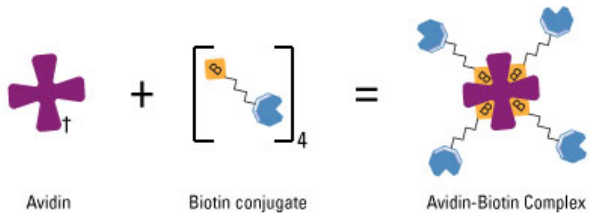

Figure 2.1. Attachment of biotin molecules to an avidin molecule. Four bonding sites are present in each avidin molecule. This image was reproduced from Sigma Aldrich.

The biotin and avidin coated particles were both purchased from Spherotech (SVFM-100-4 and TM-60-5). To generate microswimmers, avidin and biotin coated beads were

suspended (2 ul each) inside a 1 ml tube containing a synthetic mucus formulation of 1 ml volume. This solution was then vortexed for two minutes to ensure the particles were thoroughly distributed. This process is demonstrated visually in Figure 2.2. due to the randomness of this process sometimes microswimmers of more than three beads are formed and sometimes no binding occurs at all. In practice, three beads is the minimum geometric requirement for swimming in Newtonian fluids, since it possess no more than two planes of symmetry.

Figure 2.2. Fabrication of achiral microswimmers using avidin and biotin coated particles. After vortexing three bead swimmers are formed, but so are larger aggregates, as well as two bead and one bead structures.

2.2. Synthetic Mucus Formulation

Human mucus is both physiologically and rheologically complex because of its chemical formulation. Mucus is primarily composed of mucin glycoproteins, lipids, salts, DNA, cells, and cellular debris [22]. Each component effects the viscoelastic properties of mucus, even in slight concentration changes. Human samples are difficult to store for prolonged periods of time and can vary greatly from person to person. For these reasons, human mucus is often not used for scientific research where high levels of repeatability are necessary. One group has tried to formulate synthetic mucus with high degrees of success [6] but it is still a developing field of study. For this paper, a much simpler form of synthetic mucus was fabricated by rehydrating mucin glycoproteins from a porcine stomach.

Mucin glycoproteins are the most important component contributing to mucuss viscoelastic properties [22]. When hydrated in water, the protein creates a structured heterogeneous mesh fiber network [22]. Like Methyl Cellulose (MC), as concentration increases, the density of the fiber network increases as well as its overall viscosity [27]. Like other structured fluids, nanoscale particles can diffuse between the mesh fibers and ignore otherwise extreme bulk fluidic properties [22]. Larger microparticles will become trapped and entangled within the structure, leading to increased fluidic interaction. For visualization of the mesh fibers, Figure 2.3 shows clearly the fibers and the associated voids.

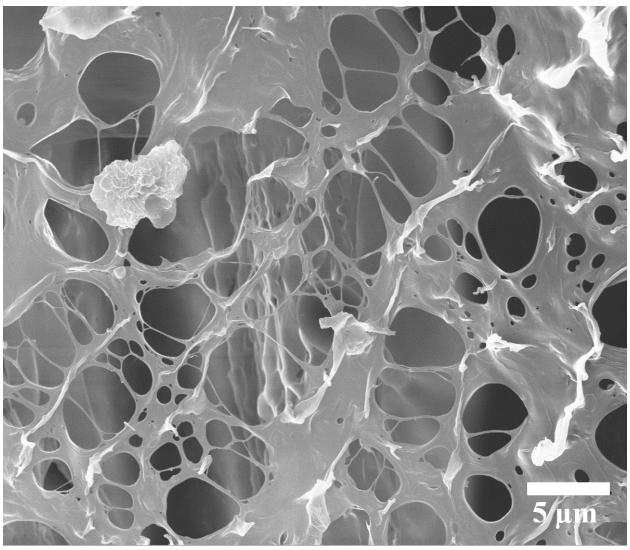

Figure 2.3. SEM image of synthetic mucus formulation. Mucin glycoprotein fibers and voids are clearly visible.

The procedure to fabricate this synthetic mucus will be outlined in this paragraph, where 4% mucin will be used as an example. Synthetic mucus of 4% concentration by weight was fabricated by mixing mucin from a porcine stomach (Type II, Sigma Aldrich) with deionized water. First 100 ml of deionized water is added to a beaker with a stirring rod. The magnetic stirrer was set to 1500 Hz and the hot plate temperature was set to 35°C. Six grams of mucin was then added to the beaker. Once all of the mucin was sufficiently wetted, an additional 50 ml of deionized water was added to the beaker. After 30 minutes, the mucin formulation

was then centrifuged for 10 minutes at 3000 rcf; this was done to remove any undissolved particulates and allow for easy viewing with an optical microscope.

To characterize the synthetic mucus formulations, a Discovery Rheometer Hybrid (DHR-3) Rheometer was used. A 40 mm flat plate was used to perform a simple shear rate test from shear rates of 0-100 $1/s$. Mucus was formulated using the above procedures at concentrations of 0.5 to 10%. Each sample was tested three times and then averaged together. Figure 2.4 shows the viscosity vs. shear rate curves for each of the samples tested. As can be seen, there is a very noticeable upward shift in the viscosity curves as the concentration of mucin is increased. Each curve also displays a shear thinning effect as shear rate increases. There is some overlap in the data at low shear rates for low concentrations; this is caused by internal flows within the water and disappears at higher mucin concentrations. For the majority of the experiments performed, 4% mucin samples were used. This concentration was selected because microrobot sedimentation by gravity was extremely slow, allowing for repeatable experiments to take place. A graph isolating the 4% mucin concentration can be seen in Figure 2.5.

2.3. Control System Setup

An approximate Helmholtz coil system was used to produce rotating magnetic fields. When a microswimmer was exposed to the fields, it would rotate about its long axis and propagate perpendicular to the rotational direction. To make a microswimmer swim omni-directionally, the approximate Helmholtz coil pairs were arrayed in the x, y, and z directions. They are approximate since the separation between each coil pair are different from those used in true Helmholtz coil design. To compensate for this discrepency, an increased voltage is applied tot eh system to force the correct magnetic field distribution at the center of the

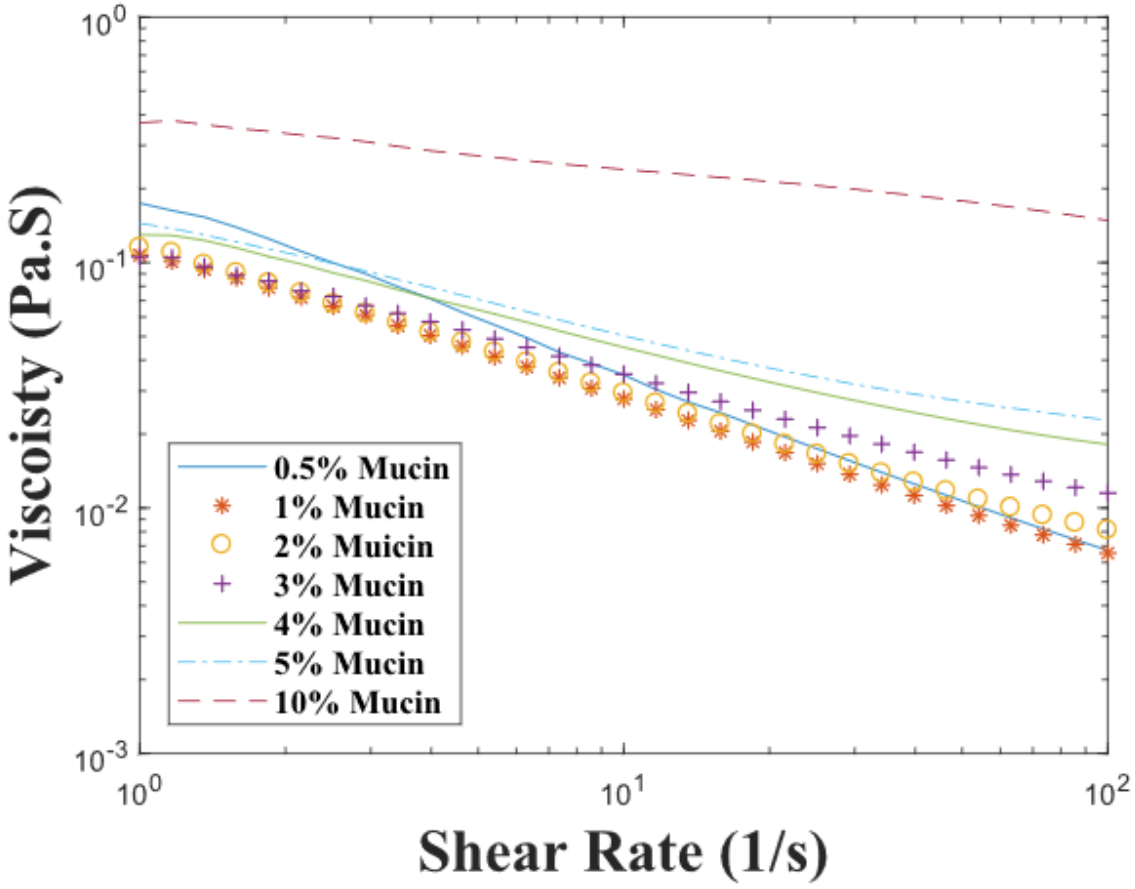

Figure 2.4. Viscosity vs. shear rate curve for different mucin concentrations. A noticable increase in overall viscosity is evident as concentration increases. Shear thinning modalities were consistent sample to sample.

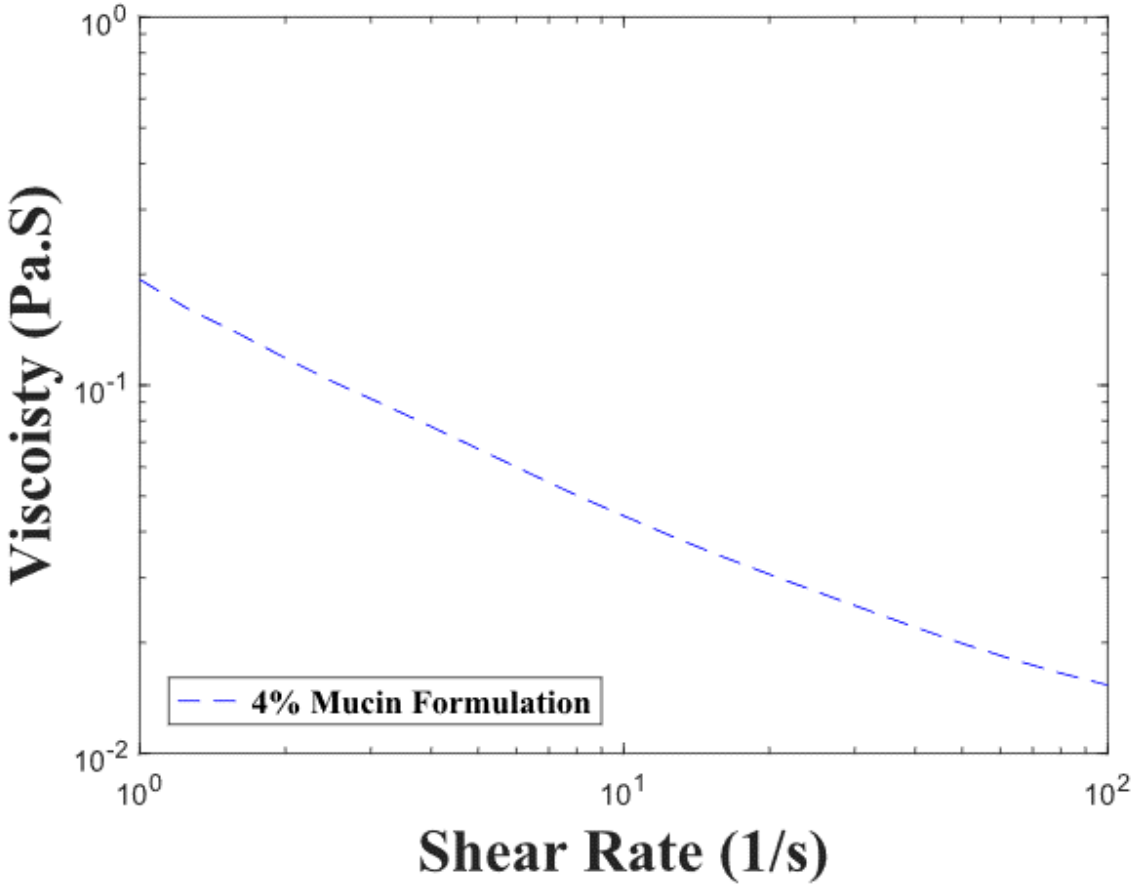

Figure 2.5. Viscosity vs. shear rate curve for 4% mucin concentration. This concentrations was used for the majority of the tests performed.

working distance. The calculations for this were performed in previous work [8].

$$B = \begin{bmatrix} -B_s \cos\theta + B_r \sin\theta \cos\omega t \\ B_s \sin\theta + B_r \cos\theta \cos\omega t \\ B_r \sin\omega t \end{bmatrix} \tag{2.1}$$

$$n = \begin{bmatrix} -\cos\theta & \sin\theta & 0 \end{bmatrix} \tag{2.2}$$

The governing equations used to generate these magnetic fields in three dimensions can be seen in equation 2.1. Where Br is the maximum amplitude of the rotating magnetic field, B_s is the magnitude of the static magnetic field, ω is the rotational frequency of the field, θ is the direction of rotation, and t is time. The static magnetic field for directional heading angle control is seen in equation 2.2. How each of the parameters discussed in equations 2.1 and 2.2 affect microrobotic swimming, can be seen in Figure 2.6. For the bulk of the experiments, the only two parameters changed were ω and θ. Magnetic field strength was designed to increase as frequency increased to modulate the microswimmers step out frequency; this was discussed in [11]. Step out frequency is when the microrobots can no longer follow the rotational magnetic fields. By modulating the field strength, the microrobots can follow the fields rotation at larger frequencies. The graph showing how field strength changes with frequency can be found in Figure 2.7.

The parameters for manipulation and control are performed using a LabVIEW program, which interfaces with external DAQ control boards to send signals to coupled bipolar power supplies. The microswimmers are observed using an inverted microscope and recorded using a CMOS camera at 30 frames per second. The centroids of the microswimmers under observation were extracted using an image processing algorithm; this will be discussed in section 2.4. An overview of the entire system set up can be seen in Figure 2.8. Microswimmers are fabricated using the method in section 2.1 and placed into a PDMS chamber 2 mm deep by 1 mm wide.

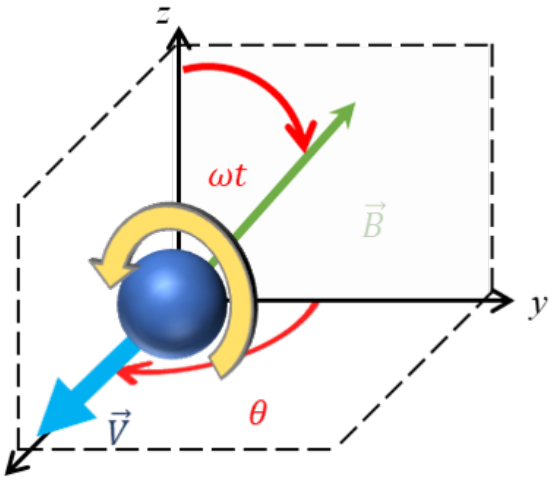

Figure 2.6. Influence of equations 2.1 and 2.2 parameters on microswimmer direction and rotational effects. The yellow arrow represents the rotation of the magnetic field.

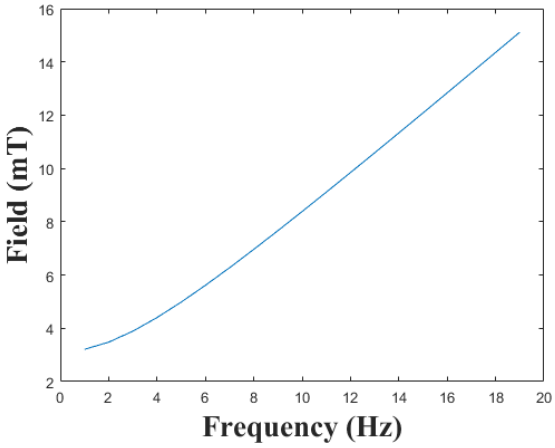

Figure 2.7. Magnetic field strength (mT) vs. Frequency (Hz) for approximate helmholtz coil system

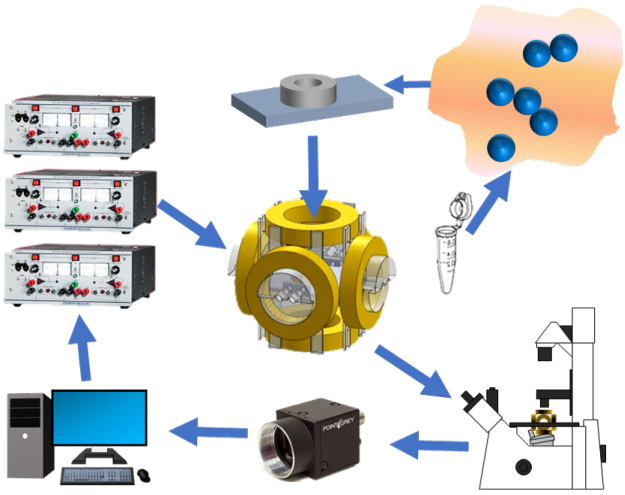

Figure 2.8. Diagram of experimental setup. The microswimmers mixed with the synthetic mucus are loaded into a PDMS chamber and placed in the center of the approximate Helmholtz coil system. Bipolar power supplies are linked to the coil system and controlled using a LabVIEW program. An inverted microscope and CMOS camera are used for visualization.

2.4. Image Processing For Microswimmer Tracking

To track the swimmer under investigation, a series of image processing techniques was utilized. Using the MATLAB image processing toolbox, each frame of a captured video would be analyzed sequentially. In the first frame the initial position of the swimmer was determined using the location of its centroid. When moving to the next frame, the position would be recalculated in reference to the previous centroids location. This is done by calculating the total change in centroid displacement using the x and y coordinates. The swimmer itself is isolated from the surrounding environment using a combination of opening, closing, and filling techniques for binary images. An example of this process can be seen in Figure 2.9. In some cases, this process was performed retroactively in LabVIEW while capturing the video, and takes place within an isolated box area localized around with microswimmer. Centroid location information was then stored in an excel spread sheet for later analysis. Additionally, other information such as heading angle, magnetic field frequency, magnetic field strength, and time are also stored in the spreadsheet.

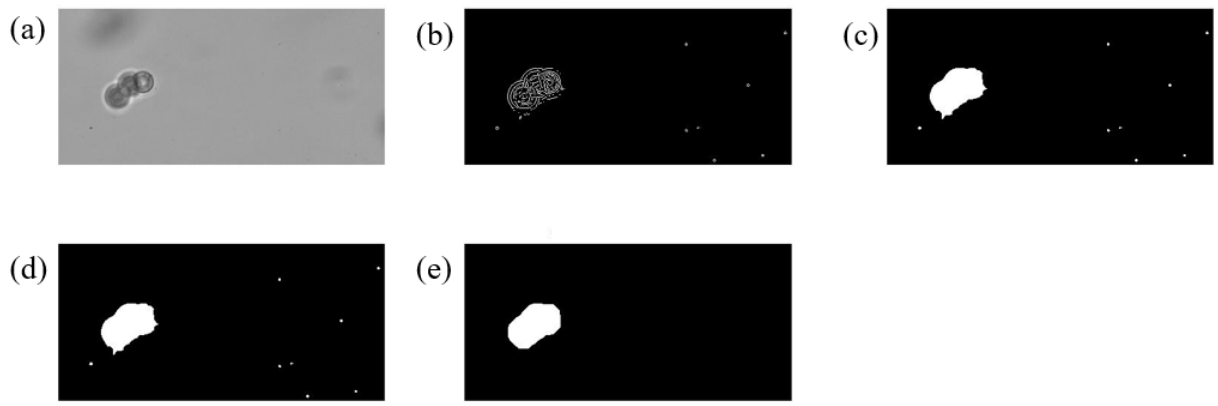

Figure 2.9. (a) captured image from CMOS camera. (b) optional edge detection of frame. (c) binary image of microswimmer. (d) opening procedure to remove any holes that may be present in the white regions. (e) closing procedure that removes any artifacts smaller than a specific size. End result of this process is a isolated microswimmer whose centroid can be tracked.

2.5. Experimental Procedure

Two types of experiments were performed in this paper. The first experiment involved increasing the magnetic field frequency from 0 to 19 Hz and determining the average velocity of the microswimmers at each frequency point. The microswimmers were tested three times and then had their frequency vs. velocity curves averaged between trials. Three bead, snowman, and single bead microswimmers were tested in this manner. Most experiments were performed using 4% mucin concentrations, with some exceptions given to three beads achiral microswimmers. The second experiment held the frequency of the microswimmers constant but varied the swimming direction of the microswimmer. In most cases, the goal was to form a simple pattern, such as a box, and compare how well it followed the trajectory.

Chapter 3

Results

3.1. Achiral Microswimmers

Achiral microswimmers, despite displaying proficient performance inside Newtonian environments, had surprising limitations when examined in synthetic mucus. The most prominent issue was that achiral three bead swimmers could not form in environments with modest to high mucin concentrations. The most likely suspicion is that swimmer formation is hindered by mucin fibers, preventing a complete avidin-biotin bond from forming. The viscous nature may also prevent aggregates of beads from forming correctly, despite prolonged agitation using a vortexer. The only microswimmers observed were only rarely found in 3% mucin concentrations. The frequency vs. velocity curve for a swimmer in 3% mucin solution can be seen in Figure 3.1, as well as its track path from post processing. However, finding these swimmers, even in a 3% concentration was extremely difficult.

At higher concentrations, achiral microswimmers became unstable. Figure 3.2 shows an example of this, where a three-bead particle breaks apart after being actuated with a 7 Hz magnetic field frequency in a 4% mucin solution. Attempting to join avidin-biotin beads together through magnetic rotation also proved to be inefficient. Figure 3.3 shows an example of this, and while larger swimmers could be formed, the only thing holding them together were magnetic attractive forces, which are not strong enough to keep the multi-bead construct together. Going beyond a 4% mucin concentration, amplified this problem, and resulted in very few achiral microswimmers being naturally formed. After, the swimmer in Figure 3.2 broke apart however, a two-bead derivative and a single particle continued traversing the environment unabated. This is curious since it should not be possible for these constructs to swim so efficiently; with both lacking chirality and flexibility. At first it was

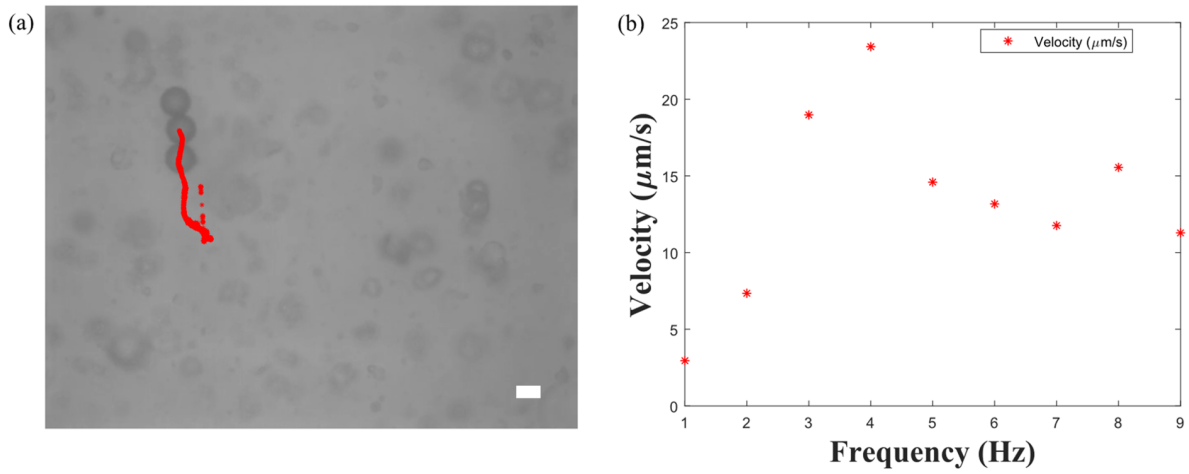

Figure 3.1. (a) Three bead achiral microswimmer track path from the start position to the final position shown. Some data points are outliers caused by issues with the tracking program. (b) velocity vs. frequency graph of the swimmer, data is heavily unreliable. The scale bar shown is 10 μm.

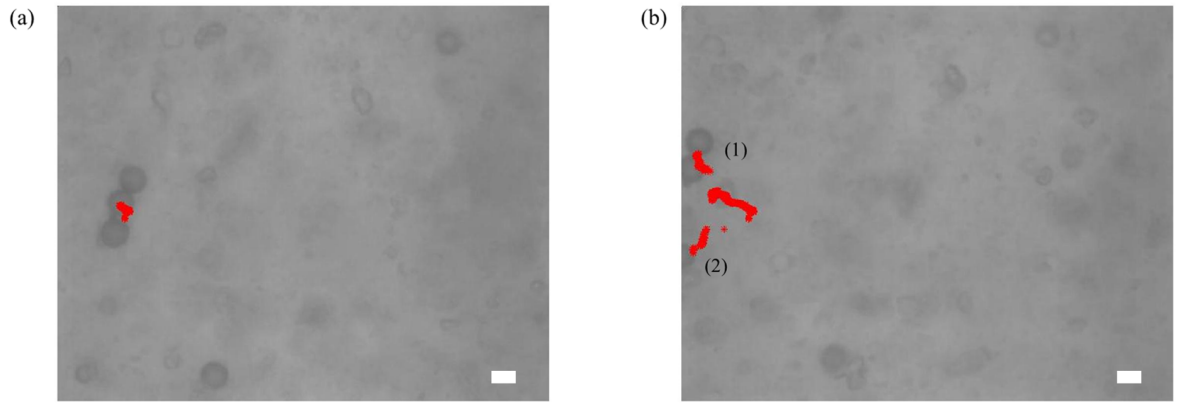

Figure 3.2. (a) Three bead achiral microswimmer beginning it's velocity vs. frequency sweep. (b) at 7 Hz the microswimmer broke into a two bead swimmer (1) and a tailed single bead swimmer (2). The cause of this failure was improper avidin-biotin chemical bonding. This is only one of several swimmers that failed in a similar manner. The scale bar shown is 10 μm.

believed that they were swimming due to a mucin tail that was attached to the constructs; Figure 3.4 is an example of this as well as the corresponding track path. However, after further investigation, numerous examples of both double bead and single bead swimmers, without added features, became more apparent. The following sections will discuss these swimmers in detail. Three bead swimmers were rare, unstable, and had inconsistent velocity results in solution.

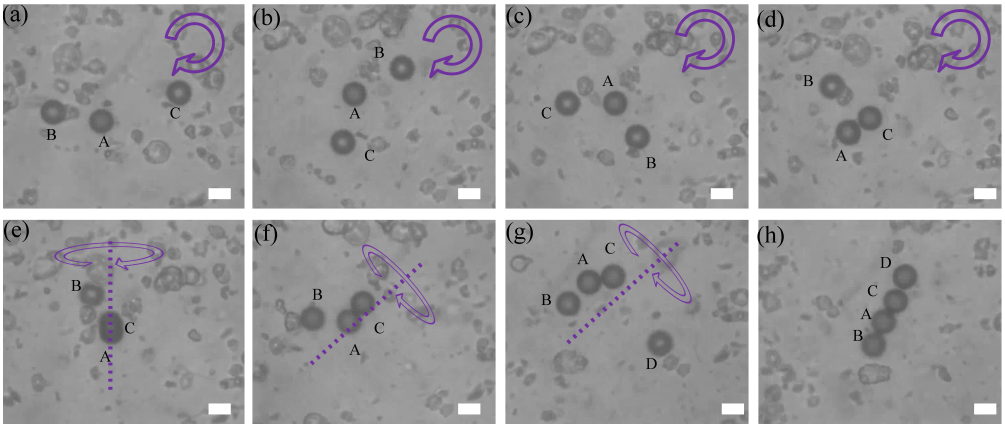

Figure 3.3. Formation of a four bead microswimmer using x-y rotating magnetic fields. (a-d) particles undergo clockwise rotation and start aggregating. (e-f) snowman swimmer forms forms. (g) achiral three bead swimmer forms. (h) four bead microswimmer forms. Only magnetic forces are keeping this swimmer together and is not stable for prolonged periods of time. The scale bar shown is 10 μm.

3.2. Snowman Microswimmers

The results of snowman microswimmers were far more promising than those of three bead microswimmers. The first conclusion was that snowman swimmers can swim through synthetic mucus mediums, despite their symmetric geometry. Figure 3.5 shows the directional controllability; (a) shows a box pattern while (b) shows an up-right-up pattern. While the intention of (a) was to create a perfect box, that was clearly not the result; the slanted trajectory was caused by slight internal flows from the snowman interacting with mucin fibers. This offset was always parallel to the direction of the rotating magnetic fields. The intention

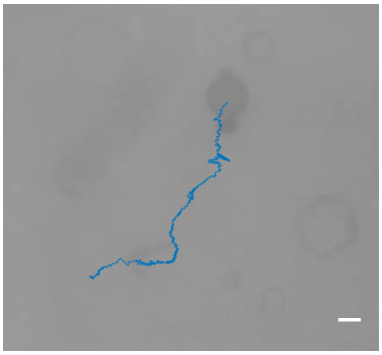

Figure 3.4. Tailed single bead particle propogating through a 5% concentration synthetic mucus environment. The scale bar shown is 10 μm.

of (b) was to create a step like appearance, but it ended up being more of a zig-zag because of the offset. During testing, a separated two bead microswimmer behaved in a much similar manner to the snowman swimmers. The separation was caused by mucin fibers entangled between the two particles. A small sample of its path planning can be seen in Fig. 3.5 (c). The separation between the beads would slightly contract when not exposed to magnetic fields. When a change in direction was performed, the swimmer would flip along its long axis and reorient itself to the correct dipole orientation. While these separated swimmers were rare, they never the less show the versatility of natural microswimmers that can be formed in such environments.

The second set of tests revolved around understanding how snowman swimmers responded to increasing rotational frequency under a constant directional input. The results of this experiment were surprising, instead of a noticeable step out frequency, the snowman swimmers maintained a linear trend in velocity as frequency increased. During some trials, a slight internal flow was present in the surrounding medium, pushing the particles the left at a constant rate of 0.8 $\mu m/s$. The microswimmers in all three trials were able to overcome this flow after about 7 Hz and propagate to the right. The results of three trials of the same snowman swimmer can be seen in Fig. 3.6 (b) where (a) is visualization of one of the trials. With slight variations, these results were repeatable among other snowman swimmers

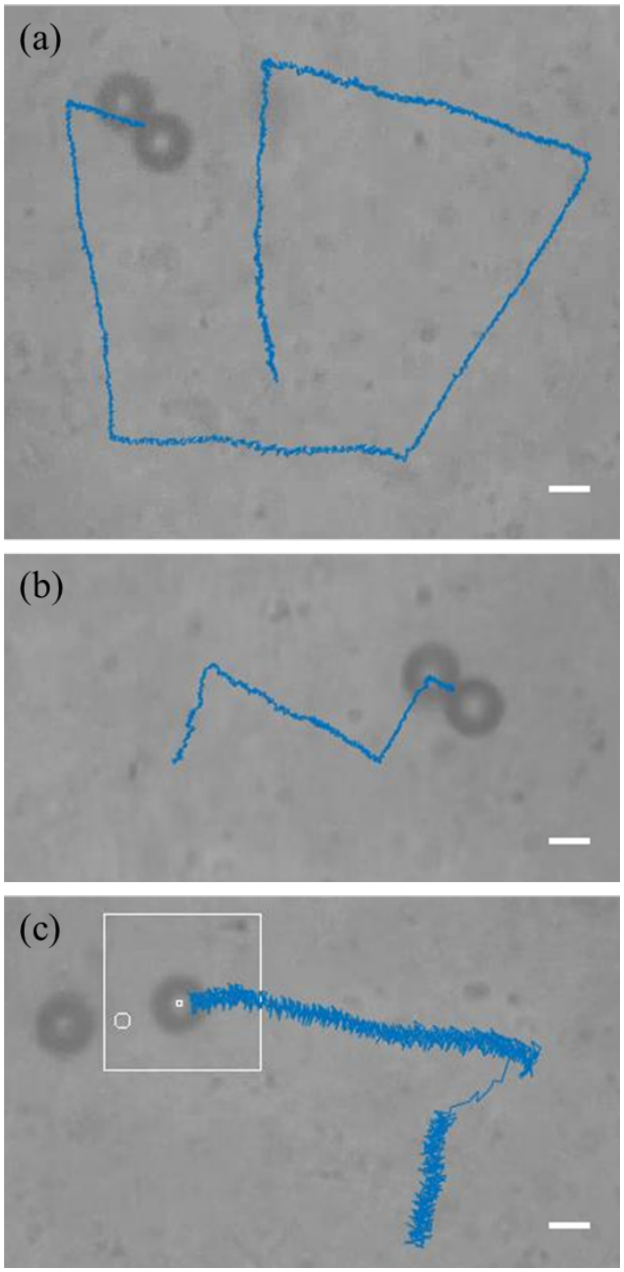

Figure 3.5. (a) a box like pattern with the swimmer moving 90°, 0°, 270°, 180°, 90°, then 180° back to the start position. The frequency during this experiment was 19 Hz. The box like pattern is visible, but due to internal flows caused by the rotation of the swimmer, the path is skewed towards the direction of rotation. (b) a step like pattern, but for the same reasons as (a), the path was skewed. Both (a) and (b) demonstrate significant directional controllability of double bead entangled swimmers. (c) shows the path of a non-contact double bead swimmer, while much rarer then the ones in (a) or (b), this swimmer was still surprisingly viable in the fluidic medium, and could be controlled just as well as its counterparts. The scale bar in (a), (b), and (c) is 10 μm.

suspended in the fluid. Lastly, multiple two bead swimmers were analyzed and compared. While no two swimmers really behave identically, very clear trends could be extracted several of the tests. Figure 3.7 shows the velocity vs. frequency curves for two snowman swimmers.

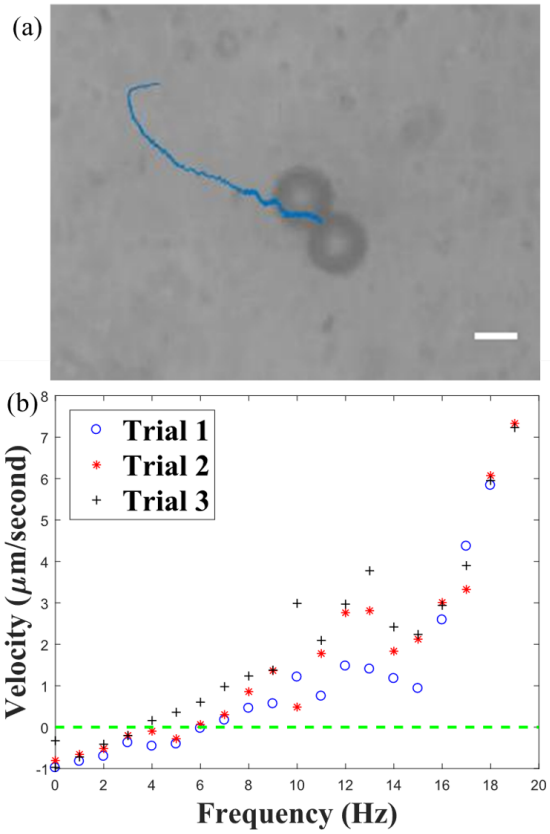

Figure 3.6. (a) shows the path of a snowman swimmer moving to the right. The initial reverse motion was caused by an internal flow of 0.8 $\mu m/s$ to the left. (b) shows the trials conducted on the swimmer, all of which show consistent upward trends. The green line represents the point where the swimmer reached equilibrium with the internal flow. The scale bar is 10 μm.

3.3. Single Bead Microswimmers

Within each mucin sample, roughly 40% of the beads investigated could be manipulated in a significant way; the rest were trapped within localized mucin concentrations. When exposed to a rotating magnetic field, the bead would travel along in the direction of the

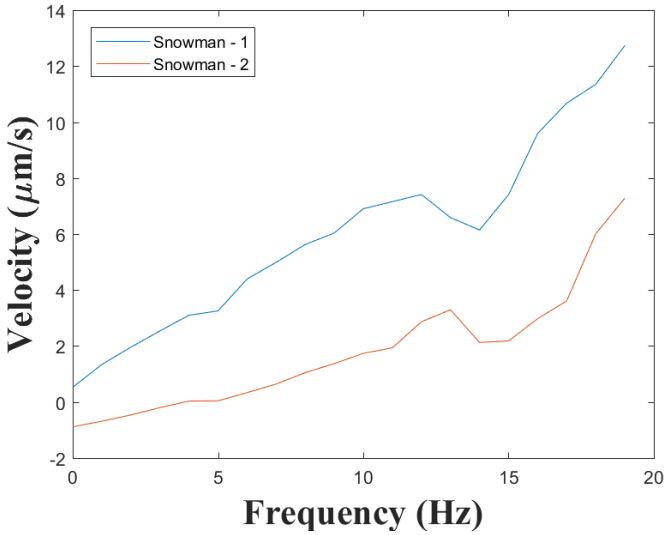

Figure 3.7. Comparison of two snowman swimmers velocity vs. frequency curves. Both are linear, and show a possible step out frequency around 14 Hz. Snowman-2 was one of the swimmers experiencing the internal flow of 0.8 $\mu m/s$.

static magnetic field, while spinning around its axis. An example of this experiment can be seen in Figure 3.8. The repeated trials of a single particle can be seen in Figure 3.9 (a). Between the three trials of this bead, performance was relatively consistent, with only one or two divergent data points. It is clear from here that as the frequency of the magnetic field rotation increases, so too does the speed of the particle. However, as the frequency was increased beyond 10 Hz, the velocity of the particle would start to become nonlinear. After performing the same set of experiments between multiple beads, the same non-linear trend continued to be observed. The average velocity vs. frequency curves between different beads can be seen in Figure 3.9 (b). The beads all appear to follow the same general type of non-linear curve, and while the velocity of individual particles between trials is consistent, the performance between different particles vary significantly. The fastest particle could reach speeds of 25 $\mu m/s$ at 19 Hz while the slowest particle could only go to around 10 $\mu m/s$. The most likely explanation for these discrepancies are that they are caused from the non-homogenous nature of synthetic mucuss fiber network. Depending on the heterogeneity

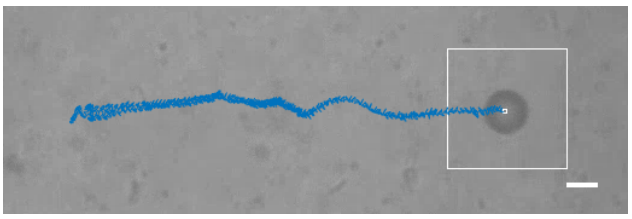

Figure 3.8. Single particle undergoing a velocity vs. frequency experiment. The frequency is incremented between 1 to 19 Hz and was tracked over time. The particle started on the left-hand side of the image and ended at the position shown on the right. The blue line shows the track path of the particles centroid throughout the test. The scale bar shown is 10 μm.

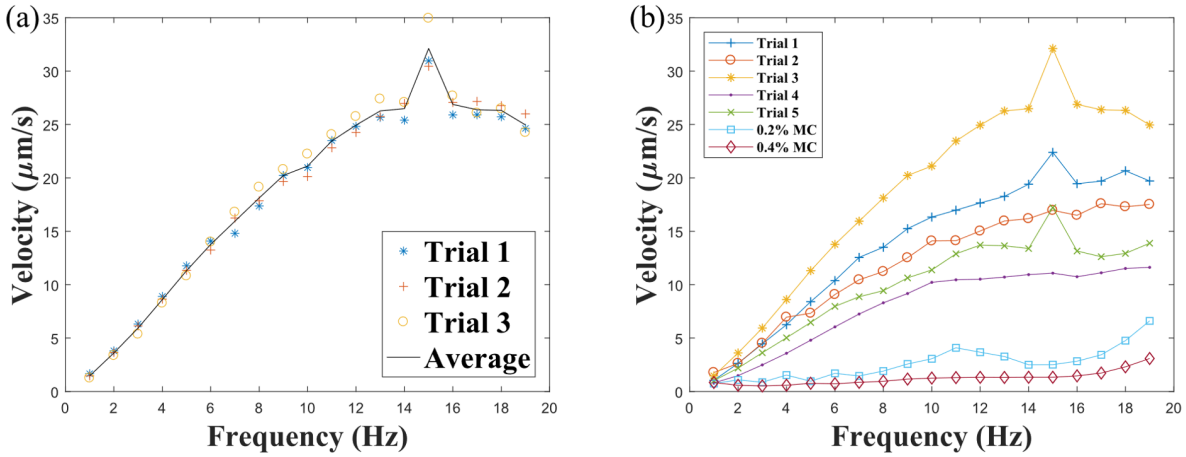

Figure 3.9. (a) Velocity vs. Frequency curve for a single particle. Between multiple trials, the velocity at each frequency was consistent. At 15 Hz there was a spike in the velocity. This happened with different beads as well. (b) shows the average velocity vs. frequency for different particles analyzed using the velocity vs. frequency experiment. Each bead had its own unique curve it followed, usually without significant deviation between trials. These differences are a combination of spatial differences in synthetic mucus and magnetic differences between beads. Each trial shows that the magnetic particles all follow the same general non-linear trend. The tests performed in methyl cellulose (MC) concentrations did not display a significant translational motion, instead the particle moved due to slight changes in internal flows as the particles rotated.

of the surrounding mucus, particles can move faster or slower than their counterparts located in other regions. The peaks caused in trails 1, 3, and 5 need to be investigated further, but its possible at this frequency there is increased penetration of the fiber network, or at worst, the indication of a possible step out frequency. This is the first documented case where a single particle could propagate through a fluidic environment without added features. To verify that the observed single particle swimming was unique to these synthetic mucus formulations, methyl cellulose (MC) concentrations of 0.2% and 0.4% were prepared. MC was selected because of its documented effects on improving performance of bacteria and Nano swimmers that was observed in other research [4, 27]. These MC concentrations were prepared using the standard procedure provided by Sigma Aldrich and characterized using the same rheological tests performed on the mucin samples. When compared to the 4% synthetic mucus sample, in Figure 3.10, the curves are not only similar in shape, but are also not far off in terms of their overall viscosity magnitudes. However, when magnetic particles

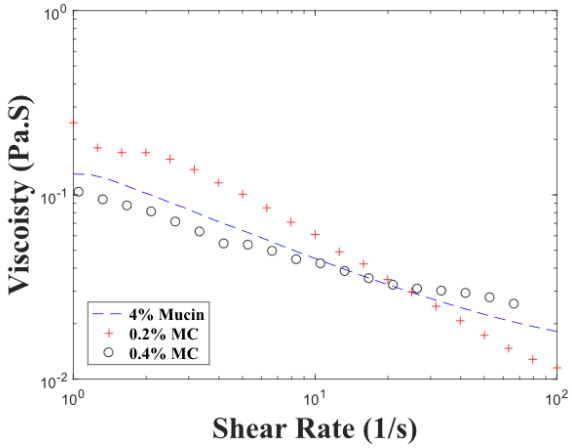

Figure 3.10. Viscosity curves for 4% synthetic mucus with 0.2% and 0.4% methyl cellulose (MC) solutions. All three curves display similar viscosity profiles, however particles were unable to move inside the MC solutions in a comparable way. The mucin fibers of the synthetic mucus created an additional interaction with the single particles to allow for translocation.

are introduced into these solutions, with the same velocity vs. frequency tests performed, there was no translational movement of the particles. The only motion on the particles

was caused directly by internal flows. The dotted lines in Figure 3.9 (b) show the averages of the tests performed in both types of MC solutions. As can be seen, with increasing concentration of MC, the particles velocity due to internal drift is reduced. Even though the MC solutions and the 4% synthetic mucus had similar viscosity curves, the beads did not perform similarly inside the MC solutions. The differences in motion must be a result of the more heterogeneous structure of the mucin fiber network inherent to the mucus solutions.

The second set of tests performed involved having a single magnetic particle swim in a square pattern. The field frequency was fixed at 19 Hz, while the magnetic field directions were altered. One test can be seen in Figure 3.11, where the red arrows represent the desired

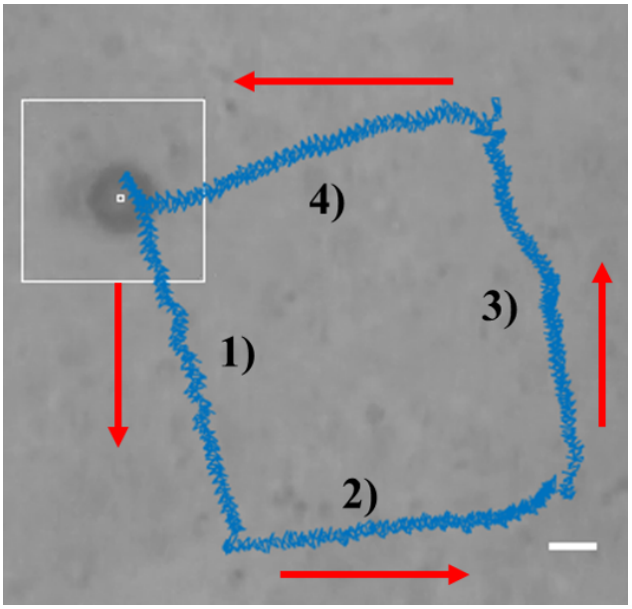

Figure 3.11. this figure shows the intended path of the particle (red arrows) compared with the actual path (blue line). The slight difference was caused by the particle rotating through the mucin along the direction of rotation. The frequency of the magnetic field was fixed at 19 Hz. The direction of the magnetic field applied was 1) 90°, 2) 0°, 3) 270°, 4) 180° respectively. The magnetic polarity of the particle was flipped only along the y-axis in this experiment. The scale bar shown is 10 μm.

trajectory, while the blue line shows the actual trajectory the particle traveled. This slight offset was the result of internal flows and of the magnetic particle wiggling itself through the

mucin sample. When examining the track path of the particle, we can see that the particle does indeed shift back and forth in Figure 3.12 (a). Despite this, the particle is still able to translate in the desired direction. When analyzing the spatial effects, the surrounding mucin has on particle velocity, we see that direction of the swimmer does indeed play a role in its performance; in Figure 3.12 b), the velocities of the particle are plotted depending on the direction it was commanded to follow. While the velocities in the 0°, 90°, and 270° directions were all similar, the 180° position was noticeable faster by about 3 $\mu m/s$. These spatial differences were further observed after multiple trials. It is important to note that

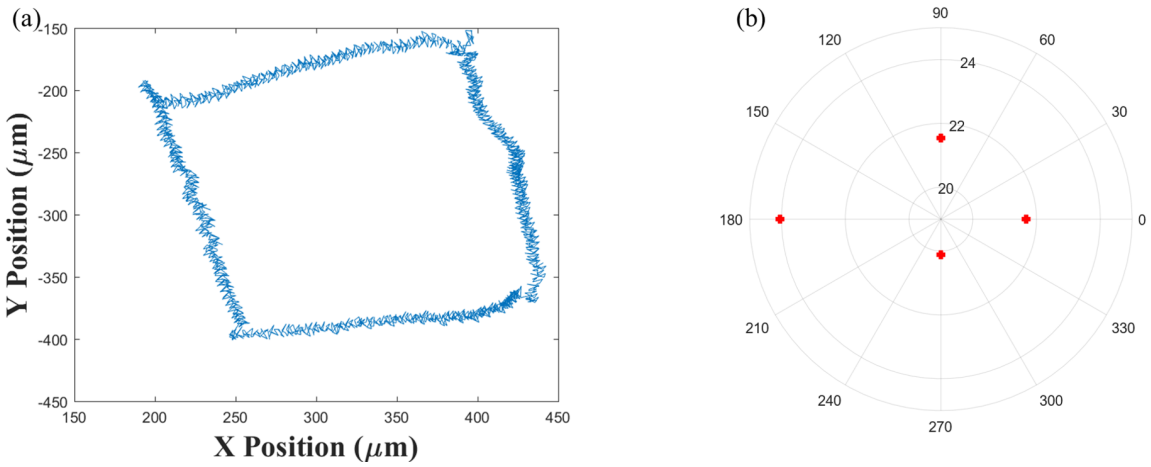

Figure 3.12. (a) shows the path the particle centroid from Figure 3.11 during the experiment. There was a slight oscillation of the particle is it progressed through the desired trajectory. (b) shows the spatial velocity dependence of the synthetic mucus as the particle moved along the desired direction. While the velocities varied slightly along 0°, 90°, and 270°; the velocity at 180° was about 3 $\mu m/s$ faster than the other directions.

during this experiment, the magnetic dipole of the particle was inconsistent. When ordered to swim in the 90° direction, it actually swam in the 270° direction. This was common among several particles analyzed during these tests. This inconsistency however, leads to a host of interesting applications, most importantly swarm control of multiple particles. The track path of two particles exposed to the same magnetic field can be seen in Figure 3.13. One common issue in microrobotics is trying to have different microswimmers behave differently

under the same magnetic field input. This was difficult to achieve in randomly formed achiral microswimmers, but with single particles it seems to be a much more common occurrence. Taking advantage of these properties could allow for novel improvements in obstacle particle computation and other input dependent applications.

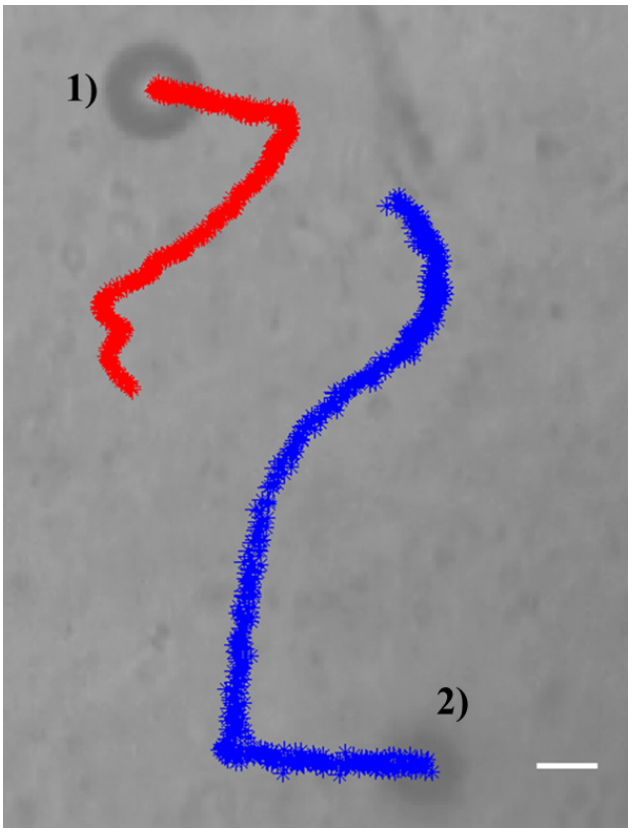

Figure 3.13. Two magnetic particles moving in similar but opposite directions. Both particles started at the center of the image. A magnetic field at 19 Hz in the 270° direction, and then after a short amount of time, a 0° direction. Particle 1) followed these commands, particle 2) went in the opposite direction due to its different magnetic handedness. The scale bar shown is 10 μm.

Chapter 4

Conclusion and Future Work

In conclusion, extremely simple aggregates of magnetic particles can be used as microswimmers in synthetic mucus environments. Three bead microswimmers were demonstrated to be rare occurrences due to avidin biotin bonding issues, while snowman and single bead particles were demonstrated to swim through the synthetic mucus environments. This is quite surprising since these structures cannot swim in Newtonian fluids. Snowman swimmers were shown to have a linear velocity vs. frequency curve and could be directionally manipulated. They were also demonstrated to be able to overcome subtle internal flows present within the medium. Single bead swimmers were shown to have a markedly increased velocity when exposed to rotating magnetic fields, but also demonstrated a nonlinear relationship which decayed at higher frequencies. Single beads could also perform simple directional manipulation to create boxes. Additionally, swarms of single particles were demonstrated to behave differently when exposed to the same control inputs, allowing for multiple particle trajectories.

Both the snowman and single particle swimmer cannot swim in Newtonian environments due to their symmetry and lack of flexibility. When placed in Methyl Cellulose (MC), another non-Newtonian fluid, single bead particles didnt display any significant swimming motion. This leads to the conclusion that the increased heterogeneity of synthetic mucus allows the aggregates to swim due to increased interactions fluidic interactions. These results indicate that snowman and single bead swimmers are viable inside human mucus environments. Single bead swimmers are perhaps the simplest microrobots ever demonstrated to propagate in biological bulk fluids. By applying a biotin labeled drug to the avidin particles, these swimmers can be used to perform targeted drug delivery applications inside the gastrointestinal tract.

Future work for this research will include performing experiments inside animal models. Rats and mice will be utilized and harvested for their mucuss and then rheologically characterized using the DHR-3 Rheometer. Both snowman and single particle swimmers will be tested for the viability in these fluidic mediums. Should these in vitro tests prove successful, in vivo tests will be performed. Fluorescence dyes will be used to help image the microswimmers inside the organs of the animals. A new large-scale Helmholtz coil system was recently constructed to carry out in vivo experiments as can be seen in Figure 4.1. Using this coil system, much larger magnetic field strengths can be generated, and a larger working space is also available to conduct experiments. It is hopeful that these microrobots can be utilized in such environments and bring significant change to the medical world.

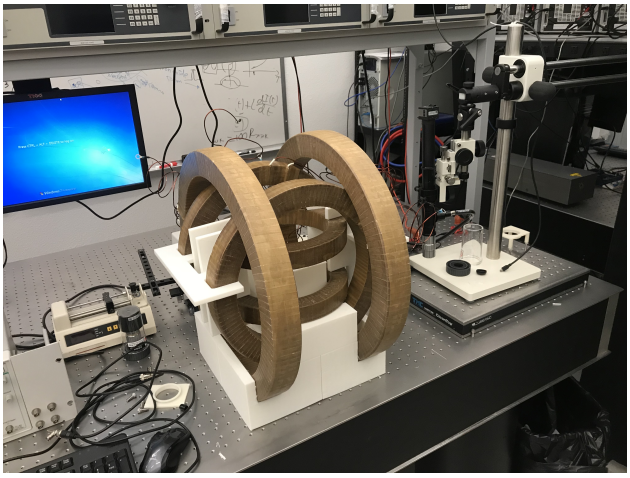

Figure 4.1. Large scale Helmholtz coil system. Total working area is 15x15 cm^2; large enough to fit a fully grown rat for observation. If 20 Amps is applied to the system, a magnetic field strength of 40 mT is possible, which is more than double the system used in this paper.

BIBLIOGRAPHY

[1] Ali, J., Cheang, U. K., Darvish, A., Kim, H., and Kim, M. J. Biotemplated flagellar nanoswimmers. *APL Materials 5*, 11 (2017), 116106. 2

[2] Ali, J., Cheang, U. K., Martindale, J. D., Jabbarzadeh, M., Fu, H. C., and Kim, M. J. Bacteria-inspired nanorobots with flagellar polymorphic transformations and bundling. In *Scientific Reports* (2017). 1

[3] Baylis, J. R., Yeon, J. H., Thomson, M. H., Kazerooni, A., Wang, X., John, A. E. S., Lim, E. B., Chien, D., Lee, A., Zhang, J. Q., et al. Self-propelled particles that transport cargo through flowing blood and halt hemorrhage. *Science advances 1*, 9 (2015), e1500379. 1

[4] Berg, H. C., and Turner, L. Movement of microorganisms in viscous environments. *Nature 278*, 5702 (1979), 349. 3, 23

[5] Boya, V. N., Lovett, R., Setua, S., Gandhi, V., Nagesh, P. K., Khan, S., Jaggi, M., Yallapu, M. M., and Chauhan, S. C. Probing mucin interaction behavior of magnetic nanoparticles. *Journal of colloid and interface science 488* (2017), 258–268. 4

[6] Burruano, B. T., Schnaare, R. L., and Malamud, D. Synthetic cervical mucus formulation. *Contraception 66*, 2 (2002), 137–140. 6

[7] Cheang, U. K., Ali, J., Kim, H., Rogowski, L., and Kim, M. J. On-surface locomotion of particle based microrobots using magnetically induced oscillation. *Micromachines 8*, 2 (2017). 1, 3

[8] Cheang, U. K., Kim, H., Milutinovic, D., Choi, J., and Kim, M. J. Feedback control of an achiral robotic microswimmer. *Journal of Bionic Engineering 14*, 2 (2017), 245 – 259. 1, 3, 11

[9] Cheang, U. K., and Kim, M. J. Self-assembly of robotic micro-and nanoswimmers using magnetic nanoparticles. *Journal of Nanoparticle Research 17*, 3 (2015), 145. 1, 3

[10] Cheang, U. K., and Kim, M. J. Fabrication and control of simple low reynolds number microswimmers. *Applied Physics Letters 109*, 3 (2016), 034101. 1, 3

[11] Cheang, U. K., Meshkati, F., Kim, D., Kim, M. J., and Fu, H. C. Minimal geometric requirements for micropropulsion via magnetic rotation. *Physical Review E 90*, 3 (2014), 033007. 2, 11

[12] Diamandis, E. P., and Christopoulos, T. K. The biotin-(strept) avidin system: principles and applications in biotechnology. *Clinical chemistry 37*, 5 (1991), 625–636.

[13] Espinosa-Garcia, J., Lauga, E., and Zenit, R. Fluid elasticity increases the locomotion of flexible swimmers. *Physics of Fluids 25*, 3 (2013), 031701. 3

[14] Fusco, S., Sakar, M. S., Kennedy, S., Peters, C., Bottani, R., Starsich, F., Mao, A., Sotiriou, G. A., Pané, S., Pratsinis, S. E., et al. An integrated microrobotic platform for on-demand, targeted therapeutic interventions. *Advanced Materials 26*, 6 (2014), 952–957. 1

[15] Gao, W., Feng, X., Pei, A., Kane, C. R., Tam, R., Hennessy, C., and Wang, J. Bioinspired helical microswimmers based on vascular plants. *Nano letters 14*, 1 (2013), 305–310. 2, 5

[16] Gmez, S., Godnez, F. A., Lauga, E., and Zenit, R. Helical propulsion in shear-thinning fluids. *Journal of Fluid Mechanics 812* (2017), R3. 3

[17] Kaynak, M., Ozcelik, A., Nourhani, A., Lammert, P. E., Crespi, V. H., and Huang, T. J. Acoustic actuation of bioinspired microswimmers. *Lab on a Chip 17*, 3 (2017), 395–400. 1

[18] Khalil, I. S., Fatih Tabak, A., Klingner, A., and Sitti, M. Magnetic propulsion of robotic sperms at low-reynolds number. *Applied Physics Letters 109*, 3 (2016), 033701. 1

[19] Kim, P. S. S., Becker, A., Ou, Y., Julius, A. A., and Kim, M. J. Imparting magnetic dipole heterogeneity to internalized iron oxide nanoparticles for microorganism swarm control. *Journal of Nanoparticle Research 17*, 3 (2015), 144. 1

[20] Kim, S., Qiu, F., Kim, S., Ghanbari, A., Moon, C., Zhang, L., Nelson, B. J., and Choi, H. Fabrication and characterization of magnetic microrobots for three-dimensional cell culture and targeted transportation. *Advanced Materials 25*, 41 (2013), 5863–5868. 1

[21] Kwon, J. O., Yang, J. S., Chae, J. B., and Chung, S. K. Micro-object manipulation in a microfabricated channel using an electromagnetically driven microrobot with an acoustically oscillating bubble. *Sensors and Actuators A: Physical 215* (2014), 77–82. 1

[22] Lai, S. K., Wang, Y.-Y., Wirtz, D., and Hanes, J. Micro-and macrorheology of mucus. *Advanced drug delivery reviews 61*, 2 (2009), 86–100. 2, 6, 7

[23] Lapa, M. F., and Hughes, T. L. Swimming at low reynolds number in fluids with odd, or hall, viscosity. *Phys. Rev. E 89* (Apr 2014), 043019. 3

[24] Lauga, E., and Powers, T. R. The hydrodynamics of swimming microorganisms. *Reports on Progress in Physics 72*, 9 (2009), 096601. 1, 2

[25] Leshansky, A. Enhanced low-reynolds-number propulsion in heterogeneous viscous environments. 051911. 3

[26] Liu, B., Powers, T. R., and Breuer, K. S. Force-free swimming of a model helical flagellum in viscoelastic fluids. *Proceedings of the National Academy of Sciences 108*, 49 (2011), 19516–19520. 3

[27] Nelson, B. J., and Peyer, K. E. Micro-and nanorobots swimming in heterogeneous liquids. *Acs Nano 8*, 9 (2014), 8718–8724. 3, 7, 23

[28] Ogrin, F. Y., Petrov, P. G., and Winlove, C. P. Ferromagnetic microswimmers. *Physical review letters 100*, 21 (2008), 218102. 1

[29] Purcell, E. M. Life at low reynolds number. In *Physics and Our World: Reissue of the Proceedings of a Symposium in Honor of Victor F Weisskopf* (2014), World Scientific, pp. 47–67. 1

[30] Qiu, T., Lee, T.-C., Mark, A. G., Morozov, K. I., Muenster, R., Mierka, O., Turek, S., Leshansky, A. M., and Fischer, P. Swimming by reciprocal motion at low reynolds number. *NATURE COMMUNICATIONS 5* (2014). Max Planck Press Release. 3

[31] Rajput, G., Majmudar, F., Patel, J., Thakor, R., and Rajgor, N. Stomach-specific mucoadhesive microsphere as a controlled drug delivery system. *Systematic Reviews in Pharmacy 1*, 1 (2010), 70. 4

[32] Riley, E. E., and Lauga, E. Enhanced active swimming in viscoelastic fluids. *EPL (Europhysics Letters) 108*, 3 (2014), 34003. 3

[33] Rogowski, L. W., Kim, H., Zhang, X., Sheckman, S., Kim, D., and Kim, M. J. Swimming in synthetic mucus. In *Ubiquitous Robots and Ambient Intelligence (URAI), 2017 14th International Conference on* (2017), IEEE, pp. 512–516. 1

[34] Sánchez, S., Soler, L., and Katuri, J. Chemically powered micro-and nanomotors. *Angewandte Chemie International Edition 54*, 5 (2015), 1414–1444. 1

[35] Schamel, D., Mark, A. G., Gibbs, J. G., Miksch, C., Morozov, K. I., Leshansky, A. M., and Fischer, P. Nanopropellers and their actuation in complex viscoelastic media. *ACS nano 8*, 9 (2014), 8794–8801. 3

[36] Servant, A., Qiu, F., Mazza, M., Kostarelos, K., and Nelson, B. J. Controlled in vivo swimming of a swarm of bacteria-like microrobotic flagella. *Advanced Materials 27*, 19 (2015), 2981–2988. 2

[37] Stanton, M., Trichet-Paredes, C., and Sanchez, S. Applications of three-dimensional (3d) printing for microswimmers and bio-hybrid robotics. *Lab on a Chip 15*, 7 (2015), 1634–1637. 3

[38] Teran, J., Fauci, L., and Shelley, M. Viscoelastic fluid response can increase the speed and efficiency of a free swimmer. *Phys. Rev. Lett. 104* (Jan 2010), 038101. 3

[39] Tottori, S., Zhang, L., Qiu, F., Krawczyk, K. K., Franco-Obregón, A., and Nelson, B. J. Magnetic helical micromachines: fabrication, controlled swimming, and cargo transport. *Advanced materials 24*, 6 (2012), 811–816. 1

[40] Williams, B. J., Anand, S. V., Rajagopalan, J., and Saif, M. T. A. A self-propelled biohybrid swimmer at low reynolds number. *Nature communications 5* (2014), 3081. 1

[41] Yu, T. S., Lauga, E., and Hosoi, A. E. Experimental investigations of elastic tail propulsion at low reynolds number. *Physics of Fluids 18*, 9 (2006), 091701. 1